Atp6i-deficient mice exhibit severe osteopetrosis due to loss of osteoclast-mediated extracellular acidification

Yi-Ping Li[1,2], Wei Chen[1], Yuqiong Liang[1], En Li[3] & Philip Stashenko[1,2]

Solubilization of bone mineral by osteoclasts depends on the formation of an acidic extracellular compartment through the action of a V-proton pump that has not yet been characterized at the molecular level[1–3]. We previously cloned a gene (*Atp6i*, for V-proton pump, H^+ transporting (vacuolar proton pump) member I) encoding a putative osteoclast-specific proton pump subunit, termed OC-116kD (ref. 4). Here we show that targeted disruption of *Atp6i* in mice results in severe osteopetrosis. *Atp6i*$^{-/-}$ osteoclast-like cells (OCLs) lose the function of extracellular acidification, but retain intracellular lysosomal proton pump activity. The pH in *Atp6i*$^{-/-}$ liver lysosomes and proton transport in microsomes of *Atp6i*$^{-/-}$ kidney are identical to that in wild-type mice. *Atp6i*$^{-/-}$ mice exhibit a normal acid-base balance in blood and urine. Our results demonstrate that *Atp6i* is unique and necessary for osteoclast-mediated extracellular acidification.

We generated a targeted deletion of exons 2–5 of *Atp6i* using embryonic stem (ES) cells (Fig. 1*a*). Mice heterozygous for the *Atp6i* mutation appeared phenotypically normal. The *Atp6i* genotypes of offspring derived from a heterozygote intercross are shown (Fig. 1*b*). We performed northern-blot and immunocytochemical staining analyses. A transcript of approximately 2.7 kb was present in the wild-type OCL RNA preparation. No signal was detected in preparations of *Atp6i*$^{-/-}$ OCLs (Fig. 1*c*). Expression of *Atp6i* was detected in wild-type tibial osteoclasts (Fig. 1*d*), but was absent in *Atp6i*$^{-/-}$ tibial osteoclasts (Fig. 1*e*). These results confirmed the null mutation of *Atp6i*.

We genotyped 93 F2 newborns, 171 three-week-old and 324 five-to-eight-week-old offspring. All newborn litter sizes were normal. The genotypic distributions of newborn and three-week-old mice were consistent with the expected frequency of mendelian segregation. In contrast, no *Atp6i*$^{-/-}$ mice survived up to the fifth week. *Atp6i*$^{-/-}$ mice had approximately 70% less body weight than their littermates at 23 days of age (Fig. 1*f*,*g*).

X-ray analysis showed that *Atp6i*$^{-/-}$ mice have shortened limbs and lack incisors and molars compared with normal littermates (Fig. 2*a*). Increased bone density was apparent in all bones (Fig. 2*a*–*c*). The histology of mutant long bones revealed an abundance of bone and cartilage trabeculae, obliterating more than

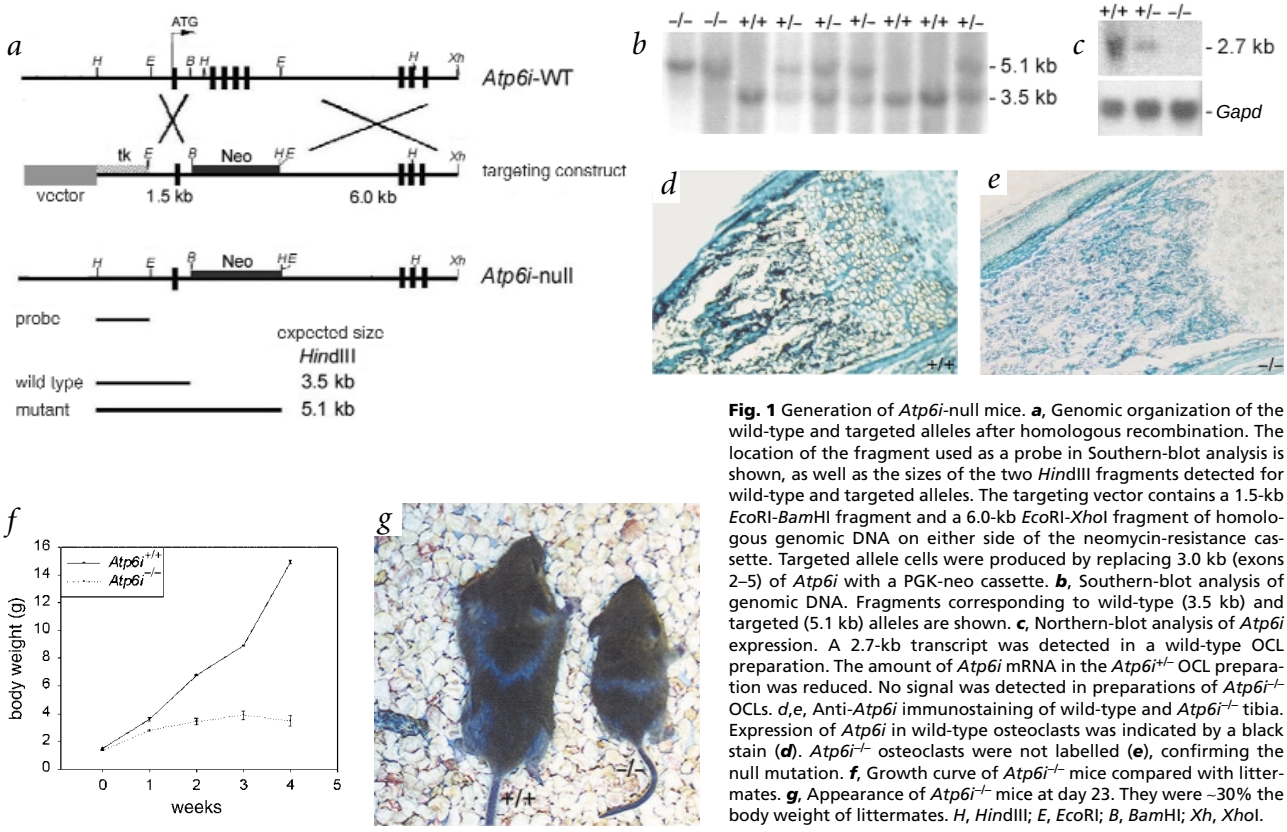

Fig. 1 Generation of *Atp6i*-null mice. ***a***, Genomic organization of the wild-type and targeted alleles after homologous recombination. The location of the fragment used as a probe in Southern-blot analysis is shown, as well as the sizes of the two *Hin*dIII fragments detected for wild-type and targeted alleles. The targeting vector contains a 1.5-kb *Eco*RI-*Bam*HI fragment and a 6.0-kb *Eco*RI-*Xho*I fragment of homologous genomic DNA on either side of the neomycin-resistance cassette. Targeted allele cells were produced by replacing 3.0 kb (exons 2–5) of *Atp6i* with a PGK-neo cassette. ***b***, Southern-blot analysis of genomic DNA. Fragments corresponding to wild-type (3.5 kb) and targeted (5.1 kb) alleles are shown. ***c***, Northern-blot analysis of *Atp6i* expression. A 2.7-kb transcript was detected in a wild-type OCL preparation. The amount of *Atp6i* mRNA in the *Atp6i*$^{+/-}$ OCL preparation was reduced. No signal was detected in preparations of *Atp6i*$^{-/-}$ OCLs. *d*,e, Anti-*Atp6i* immunostaining of wild-type and *Atp6i*$^{-/-}$ tibia. Expression of *Atp6i* in wild-type osteoclasts was indicated by a black stain (***d***). *Atp6i*$^{-/-}$ osteoclasts were not labelled (***e***), confirming the null mutation. ***f***, Growth curve of *Atp6i*$^{-/-}$ mice compared with littermates. ***g***, Appearance of *Atp6i*$^{-/-}$ mice at day 23. They were ~30% the body weight of littermates. *H*, *Hin*dIII; *E*, *Eco*RI; *B*, *Bam*HI; *Xh*, *Xho*I.

[1]*Department of Cytokine Biology, The Forsyth Institute, Boston, Massachusetts, USA.* [2]*Harvard-Forsyth Department of Oral Biology, The Forsyth Institute & Harvard School of Dental Medicine, Boston, Massachusetts, USA.* [3]*Cardiovascular Research Center, Massachusetts General Hospital, Department of Medicine, Harvard Medical School, Charlestown, Massachusetts, USA. Correspondence should be addressed to Y.-P.L. (e-mail: ypli@forsyth.org).*

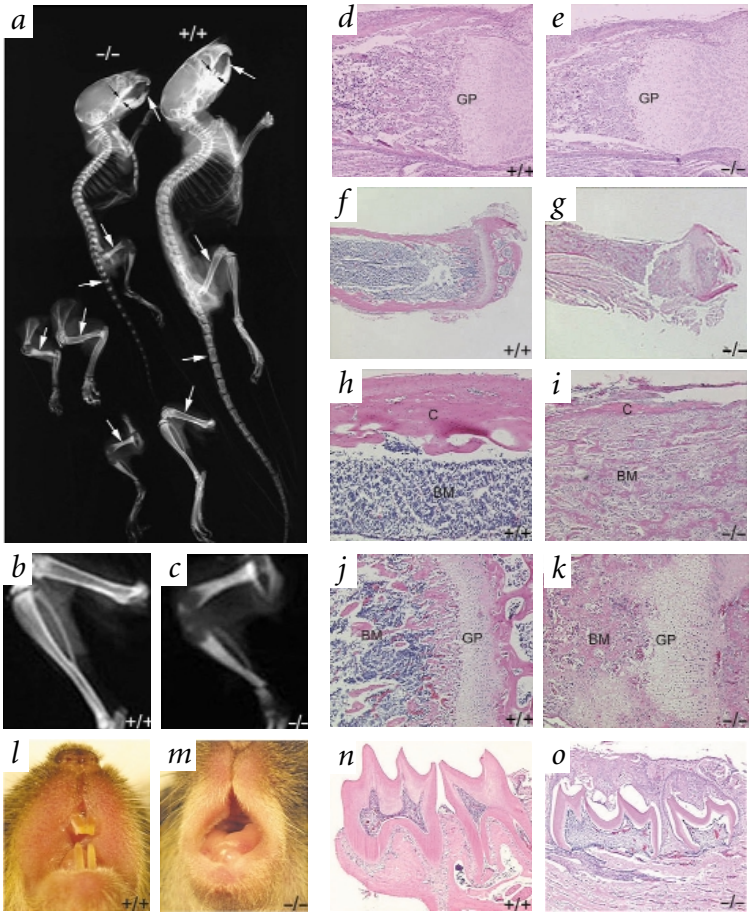

Fig. 2 Radiographic and histological analysis of *Atp6i*$^{-/-}$ mice. ***a***, Representative radiographs of the axial skeleton and limbs of four-week-old *Atp6i*$^{-/-}$ mice. *Atp6i*$^{-/-}$ mice have shortened limbs (arrow) compared with wild-type and *Atp6i*$^{+/-}$ littermates. There is sclerosis of the tibia and caudal vertebrae in *Atp6i*$^{-/-}$ mice (arrows). Mandibular and maxillary incisors and molars are not present in *Atp6i*$^{-/-}$ mice (arrows). The increased density in *Atp6i*$^{-/-}$ is uniformly present in all bones. ***b***,***c***, High magnification of corresponding limbs in (*a*). *d–k*, Histological analysis of bone in wild-type (***d***,***f***,***h***,***j***) and *Atp6i*$^{-/-}$ littermates (***e***,***g***,***i***,***k***). *h*,*j*, High magnification of (*f*). *i*,*k*, High magnification of (*g*). The growth plates of *Atp6i*$^{-/-}$ mice at one day (*e*) and four weeks (*k*) had an extended and irregular zone of calcified cartilage compared with wild-type controls (*d*,*j*). In addition, the zone of the hypertrophic chondrocytes was increased in mutant mice (*e*,*k*). Note the abundance of calcified trabeculae present in the bone marrow cavity of four-week-old mutant mice, leading to a lack of a normal marrow cavity (*i*) compared with that of wild-type mice (*h*). The cortical bone in *Atp6i*$^{-/-}$ mice (*i*) is thin compared with that of wild-type littermates (*h*). A fracture was present in *Atp6i*$^{-/-}$ tibia (*g*). *l*,*m*, Photograph of incisor eruption in three-week-old mice. Incisors appeared in the oral cavity in normal mice (***l***), but did not erupt in *Atp6i*$^{-/-}$ mice (***m***). Histological analysis of teeth in wild-type (***n***) and *Atp6i*$^{-/-}$ (***o***) littermates is shown. A section through the maxillary molars shows complete tooth eruption in three-week-old wild-type mice (*n*), whereas the teeth in mutant mice fail to erupt because of the persistence of bone (*o*). GP, growth plate; BM, bone marrow; C, cortical bone.

80% of the marrow space (Fig. 2*g*,*i*) compared with wild-type mice (Fig. 2*f*,*h*). In addition, the cortical bone of *Atp6i*$^{-/-}$ mice was thin and fragile (Fig. 2*g*,*i*). The growth plates of one-day-old (Fig. 2*e*) and four-week-old (Fig. 2*k*) *Atp6i*$^{-/-}$ mice showed an extended and highly irregular zone of calcified cartilage compared with controls. The width of the hypertrophic chondrocyte zone in tibia of *Atp6i*$^{-/-}$ mice was increased (Fig. 2*e*,*k*). With respect to tooth development, incisors did not erupt in three-week-old *Atp6i*$^{-/-}$ mice (Fig. 2*m*). Histological analysis revealed complete tooth eruption in three-week-old wild-type mice (Fig. 2*n*), whereas the teeth in mutant mice failed to erupt because of the persistence of overlying bone (Fig. 2*o*). The phenotypes of *Atp6i*$^{-/-}$ mice derived from the two independent *Atp6i*$^{+/-}$ ES clones were identical. Necropsies revealed that all other organs were normal. *Atp6i*$^{-/-}$ mice survived up to 12 weeks when fed with the milk of foster mothers after weaning. The severe osteopetrosis in *Atp6i*$^{-/-}$ mice may thus mimic an extremely malignant form of osteopetrosis in humans, in which death occurs before one year if untreated[5].

The observed osteopetrotic phenotype may be due to failure of either osteoclast formation during development, as has been observed in mice lacking c-Fos, pU1, Nf-κb, p50 and p52 (refs 6–8), or a deficiency in osteoclast activation, as has been seen in mice lacking c-Src (ref. 9). Tartrate-resistant acid phosphatase (TRAP) staining of newborn wild-type and *Atp6i*$^{-/-}$ mouse tibia

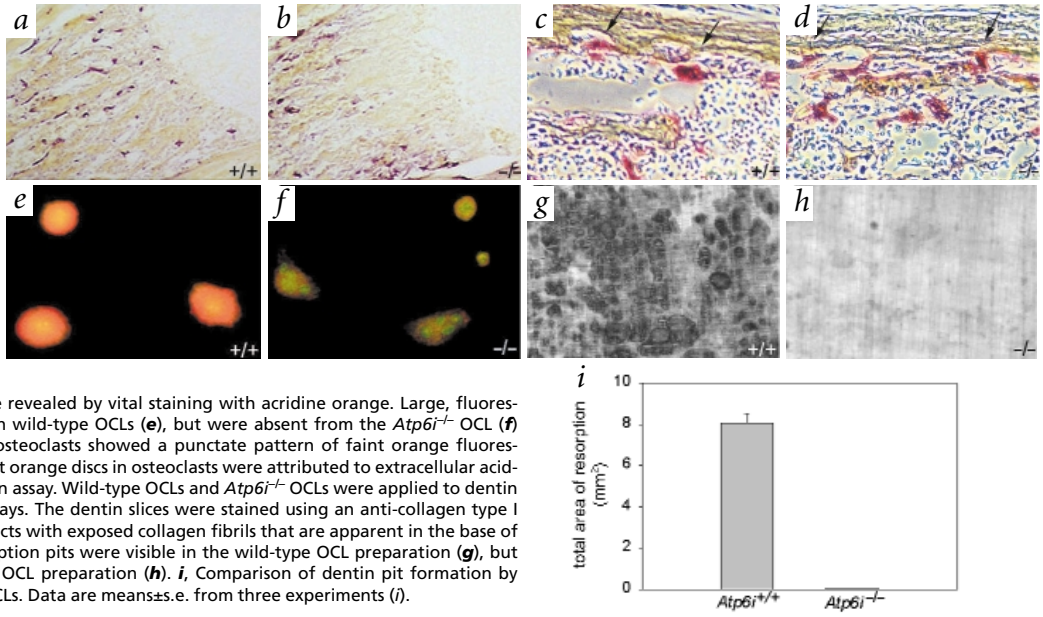

Fig. 3 The morphology and properties of wild-type and *Atp6i*$^{-/-}$ osteoclasts. TRAP staining of one-day-old wild-type (***a***) and *Atp6i*$^{-/-}$ (***b***) tibia is shown. There are no quantitative or morphologic differences between wild-type and *Atp6i*$^{-/-}$ osteoclasts. *c*, High magnification of (*a*). *d*, High magnification of (*b*). *Atp6i*$^{-/-}$ osteoclasts attached to bone but did not form lacunae (***d***, arrows), whereas wild-type osteoclasts formed lacunae (***c***, arrows). *e*,*f*, Analysis of extracellular acid compartment formation. Acid compartments were revealed by vital staining with acridine orange. Large, fluorescent orange discs were seen in wild-type OCLs (***e***), but were absent from the *Atp6i*$^{-/-}$ OCL (***f***) preparation. Rather, *Atp6i*$^{-/-}$ osteoclasts showed a punctate pattern of faint orange fluorescence (*f*). The large, fluorescent orange discs in osteoclasts were attributed to extracellular acidification. *g*,*h*, Dentin resorption assay. Wild-type OCLs and *Atp6i*$^{-/-}$ OCLs were applied to dentin slices and cultured for three days. The dentin slices were stained using an anti-collagen type I polyclonal antibody, which reacts with exposed collagen fibrils that are apparent in the base of the lacuna. Many of the resorption pits were visible in the wild-type OCL preparation (***g***), but were not seen in the *Atp6i*$^{-/-}$ OCL preparation (***h***). ***i***, Comparison of dentin pit formation by wild-type OCLs and *Atp6i*$^{-/-}$ OCLs. Data are means±s.e. from three experiments (*i*).

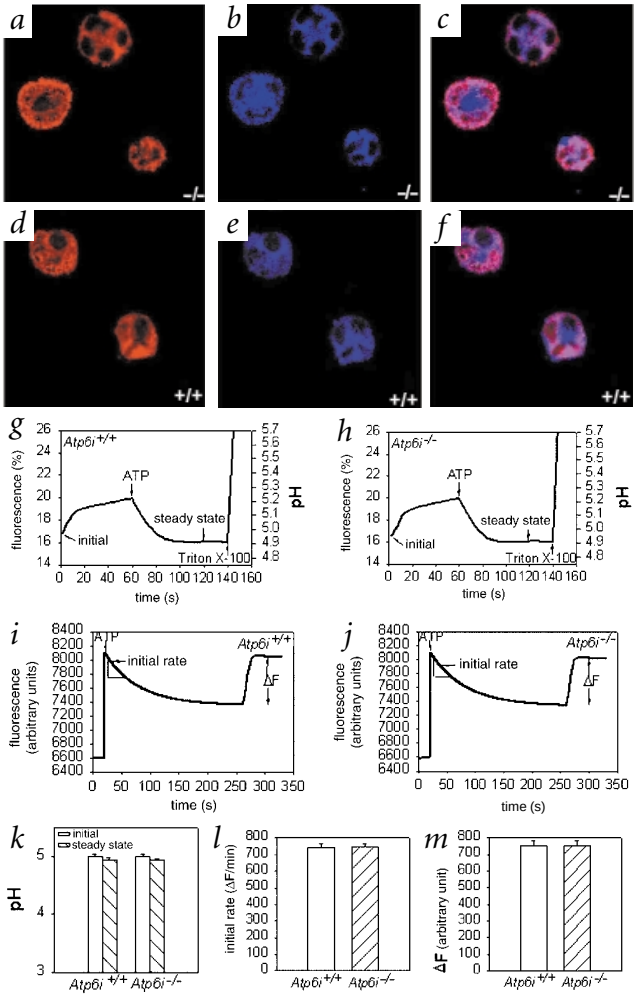

Fig. 4 The *Atp6i*-null mutation does not affect osteoclast lysosomal acidification or normal acidification in other organs. Wild-type and *Atp6i*$^{-/-}$ OCLs were stained with acridine orange on cover slips (***a***,***d***), and then immunocytochemically stained using a monoclonal antibody against to LAMP-1 (***b***,***e***), sequentially, and examined by confocal microscopy. The aridine orange staining pattern in cytoplasm of wild-type and *Atp6i*$^{-/-}$ OCLs was superimposed with the immunocytochemical staining, evident in the merged image (***c***,***f***). The intralysosomal pH in isolated wild-type (***g***) and *Atp6i*$^{-/-}$ (***h***) lysosomes was measured by determining the fluorescence spectrum of FITC-dex. The pH in both isolated *Atp6i*$^{-/-}$ and wild-type mouse liver lysosomes was about 5 at initial measurement, and gradually increased to 5.2 in assay buffer. Addition of ATP caused acidification that reached steady state at about pH 4.9 within 60 s in both *Atp6i*$^{-/-}$ and wild type. Addition of Triton X-100 disrupted the lysosomes and exposed FITC-dex to the incubation medium. Data are means±s.e. from three experiments with duplicate determinations (***k***). The initial and steady state pH in isolated lysosomes from *Atp6i*$^{-/-}$ and wild-type mouse liver were identical. *i*,*j*, Kidney microsomal proton transport assay. Proton transport in microsomal preparations derived from wild-type (***i***) and *Atp6i*$^{-/-}$ (***j***) mouse kidney was monitored as fluorescence quench of acridine orange. The initial rates of the proton flux and total acidification achieved in *Atp6i*$^{-/-}$ mouse kidney microsomal preparation were identical compared to that in the wild-type kidney microsomal preparation (*i*,*j*). Data are means±s.e. from four experiments for initial rate (***l***) and total acidification achieved (***m***).

showed neither quantitative nor morphologic differences between wild-type and *Atp6i*$^{-/-}$ osteoclasts (Fig. 3*a*,*b*), indicating that osteoclast differentiation in *Atp6i*$^{-/-}$ mice was normal. Histological analyses revealed that wild-type osteoclasts formed lacunae when they attached to bone *in vivo* (Fig. 3*c*). In contrast, *Atp6i*$^{-/-}$ osteoclasts attached but did not form lacunae (Fig. 3*d*), indicating impaired osteoclastic bone resorption.

To clarify that a defect in *Atp6i*$^{-/-}$ osteoclasts, instead of other factors *in vivo*, blocked bone resorption, we carried out *in vitro* dentin resorption assays[10] to assess the capability of *Atp6i*$^{-/-}$ osteoclasts to demineralize extracellular matrix. Many resorption pits were visible with the wild-type OCL preparation. The total area resorbed by wild-type OCLs equalled 58% of the entire surface (Fig. 3*g*,*i*). The total area resorbed by the same number of *Atp6i*$^{-/-}$ OCLs was undetectable (Fig. 3*h*,*i*), indicating that demineralization did not take place with these cells.

To further characterize the source of the deficiency in *Atp6i*$^{-/-}$ osteoclast function, we studied whether extracellular acid compartments were formed beneath the *Atp6i*$^{-/-}$ OCLs. We saw fluorescent orange discs in wild-type OCLs on cultures of dentin slices (Fig. 3*e*), but not in *Atp6i*$^{-/-}$ OCLs (Fig. 3*f*). Instead, *Atp6i*$^{-/-}$ osteoclasts showed a punctate pattern of faint orange fluorescence. We believe that the fluorescent orange discs in wild-type osteoclasts are attributable to extracellular acidification, whereas the punctate orange pattern may correspond to intracellular acidic vacuoles (for example lysosomes) within osteoclasts[2]. To confirm this, wild-type OCLs and *Atp6i*$^{-/-}$ OCLs were stained with acridine orange on cover slips, immunocytochemically stained using a monoclonal antibody against LAMP-1 (lysosomal marker; ref. 11) and examined by confocal microscopy. The punctate pattern of acridine orange cytoplasmic staining in wild-type and *Atp6i*$^{-/-}$ OCLs was identical to that of immunocytochemical staining for LAMP-1 (Fig. 4*a*,*b*,*d*,*e*), which is evident in the merged image (Fig. 4*c*,*f*). No staining was seen in the nucleus. This demonstrates that although *Atp6i*$^{-/-}$ OCLs lose the function of extracellular acidification, they appear to retain intracellular acidification, indicating the presence of more than one type of proton pump in osteoclasts.

To test whether the *Atp6i*-null mutation affects V-proton pump function in other cell types, we performed a direct measurement of acidification in lysosomal fractions prepared from liver[12]. pH-sensitive fluorescein isothiocyanate-conjugated dextran (FITC-dex) was introduced preferentially into hepatic lysosomes by intraperitoneal injection. The pH in both isolated *Atp6i*$^{-/-}$ and wild-type mouse liver lysosomes was approximately

Table 1 • Acid-base balance in the blood and urine of four-week-old *Atp6i*$^{-/-}$ and wild-type mice

	Blood (pH)			Urine (pH)		
	+/+	–/–	Diff.	+/+	–/–	Diff.
L1	7.57	7.43	0.14	6.24	6.66	–0.42
L2	7.47	7.54	–0.07	8.12	8.20	–0.08
L3	7.46	7.45	0.01	8.20	8.12	0.08
L4	7.51	7.55	–0.04	6.02	6.56	–0.54
L5	7.41	7.50	–0.09	7.30	7.23	0.07
Average	7.48	7.49	–0.01	7.16	7.37	–0.206
s.d.	0.06	0.05	0.092	1.02	0.78	0.261

Mean differences (Diff.) between genotypes in blood pH and urine pH levels were evaluated by paired *t*-tests and were not statistically significant (t_4=–0.24, *P*=0.82 for blood; t_4=–1.76, *P*=0.15 for urine).

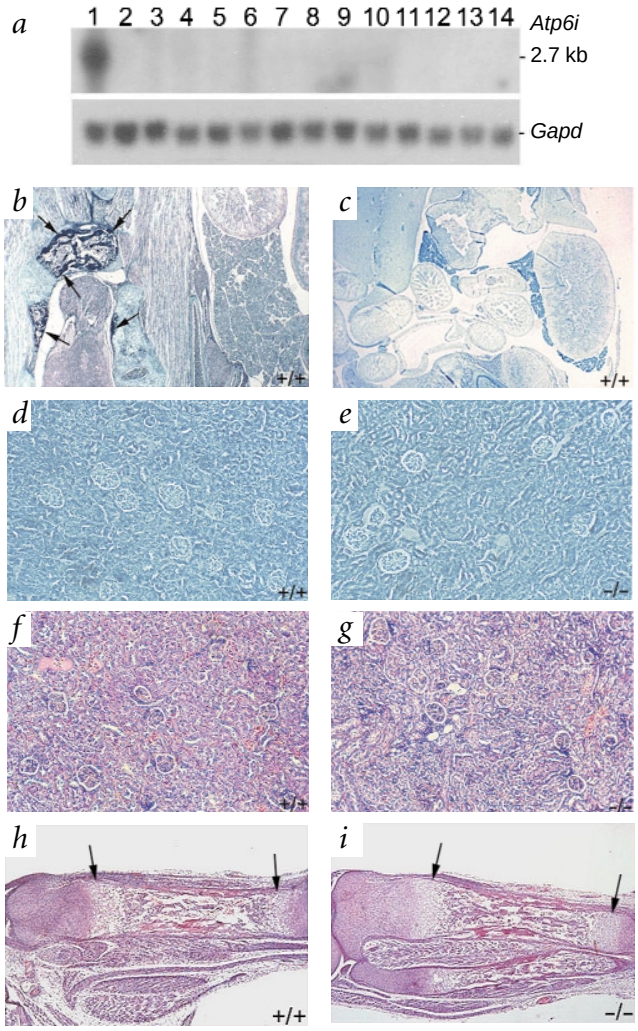

Fig. 5 Tissue and cellular distribution of *Atp6i*. ***a***, Northern-blot hybridization of human *Atp6i* cDNA probe to total cell RNA from OCLs and mouse tissues detects a 2.7-kb transcript. Total RNA (15 μg) from each tissue was blotted onto a nylon filter. Lane 1, OCLs; lane 2, testis; lane 3, brain; lane 4, skeletal muscle; lane 5, liver; lane 6, spleen; lane 7, intestine; lane 8, kidney; lane 9, thymus; lane 10, lung; lane 11, skin; lane 12, MS12 stromal cells; lane 13, undifferentiated MOCP-5; lane 14, MC-3T3 mouse osteoblast cells. ***b***,***c***, Immunocytochemical staining of newborn mouse sections using an Atp6i-specific polyclonal antibody. The antibodies intensively react with osteoclasts located in skeletal tissues, but did not react with extraskeletal tissues or cells. ***d***,***e***, The antibodies did not react with tissue sections of wild-type or *Atp6i*$^{-/-}$ kidney. ***f***,***g***, Three-week-old *Atp6i*$^{-/-}$ kidney shows normal histology, identical to that of wild type. ***h***,***i***, Comparison of bone morphology of E16 *Atp6i*$^{-/-}$ embryos with that of wild type. The zone of hypertrophic chondrocytes (arrows) in tibia of mutant mouse embryos was increased (***i***). The shape of the bone of the mutant embryo was relatively normally developed compared with that of wild-type mouse embryos.

5 at initial measurement and gradually increased in assay buffer to 5.2 (Fig. 4*g*,*h*) due to gradual alkalinization of lysosomes[12]. Addition of ATP instantly caused acidification of lysosomes from both *Atp6i*$^{-/-}$ and wild-type mouse liver that reached a steady state at approximately pH 4.9 within 60 seconds (Fig. 4*g*,*h*,*k*).

We also examined kidney microsomal proton transport in *Atp6i*$^{-/-}$ mice, which is mediated by a V-proton pump[13]. The initial rates of the proton flux and total acidification achieved in the microsomal preparation from *Atp6i*$^{-/-}$ kidney were identical compared with that in the microsomal preparation from wild-type kidney (Fig. 4*i*,*j*,*l*,*m*).

To further confirm that the null mutation of *Atp6i* did not affect kidney proton transport, we measured acid-base balance in the blood and urine of *Atp6i*-deficient mice. Blood pH exhibited minimal variation and identical mean scores for both *Atp6i*$^{-/-}$ and wild-type littermates (Table 1). Variation in urine pH was largely between litters rather than between genotypes. The mean difference between genotype in blood and urine pH levels was evaluated by paired *t*-tests and was not statistically significant. These data indicate that kidney proton transport and endosome/lysosome acidification in *Atp6i*-deficient mice are normal.

We next determined the tissue and cellular distribution of *Atp6i*. *Atp6i* was highly expressed in OCLs, but undetectable in other tissues (Fig. 5*a*). We confirmed the cell-specific expression of Atp6i by immunocytochemical staining of newborn mouse sections. The antibodies reacted with osteoclasts located in newborn mouse skeletal tissues, but not with extraskeletal tissues or cells, including muscle, intestine, skin, spleen, kidney, stromal cells or other bone marrow cells (Fig. 5*b*,*c*). No reactivity was seen in wild-type or *Atp6i*$^{-/-}$ kidney (Fig. 5*d*,*e*). In addition, three-week-old *Atp6i*$^{-/-}$ kidney had normal histology compared with that of wild type (Fig. 5*f*,*g*). We also examined bone morphology of embryonic day (E) 16 *Atp6i*$^{-/-}$ mice. The zone of hypertrophic chondrocytes in the tibia of *Atp6i*$^{-/-}$ embryos was increased (Fig. 5*i*). The shape of the bone, however, developed normally compared with that of wild-type embryos (Fig. 5*h*), suggesting that osteoclast activity is important, but not essential, during embryonic skeletal development. In this regard, blood vessel invasion of the cartilage may involve extracellular protease activity rather than osteoclast resorption[14,15].

Our work is the first to demonstrate that the osteoclast V-proton pump is structurally and functionally different from other V-proton pumps in the cell and possibly from all other known V-proton pumps. The osteoclast-specific expression of *Atp6i* and the bone-specific phenotype of *Atp6i*$^{-/-}$ mice suggest that *Atp6i* may be a useful target for therapeutic design and intervention in skeletal diseases manifesting with increased bone or cartilage resorption.

Methods

Targeting vectors. We cloned mouse *Atp6i* genomic DNA from a 129/Sv genomic library (Stratagene) and determined its genomic organization by Southern-blot analysis and DNA sequencing. To generate the *Atp6i* targeting vector, we deleted a 3.0-kb *Bam*HI-*Eco*RI fragment which contains exons 2–5 (encoding aa 25–205) of *Atp6i*, and replaced it with a PGK-neo-polyA cassette by blunt-end ligation. The PGK-thymidine kinase gene was inserted into the *Eco*RI site, 1.5 kb upstream of the *Bam*HI site. The targeting vector contained 1.5–6.0 kb of homologous genomic DNA on either side of the neomycin-resistance cassette.

Generation of *Atp6i*-disrupted mutant ES cell lines and mice. We transfected J1 ES cells with a linearized targeting vector by electroporation and selected in a medium containing G418 + FIAU as described[16]. We analysed 198 G418/FIAU-resistant ES cell clones by Southern-blot hybridization using the *Hin*dIII-*Eco*RI genomic fragment as a probe; 25 clones had a targeted allele. We injected two *Atp6i*$^{+/-}$ ES clones into C57BI/6J blastocysts to obtain chimaeric mice. Germline transmission was achieved by backcrossing with C57BL/6J inbred mice.

Genotype analysis. We prepared genomic DNA from tails as described[17]. For genotype analysis, DNA was digested with *Hin*dIII, blotted and hybridized to a genomic probe as indicated.

Preparation of OCLs and assay for dentin resorption. Spleen cells from four-week-old wild-type or *Atp6i*$^{-/-}$ mice were co-cultured with MS12 stromal cells in the presence of 10^{-8} M vitamin D_3 for 9 d as described[10]. TRAP$^+$ OCLs were enriched and pipetted onto dentin slices for dentin resorption assays. We performed dentin resorption assays as described[10,18]. Bone pits were visualized by immunostaining using an anti-collagen type I polyclonal antibody[19].

mRNA phenotypic assessment. We examined TRAP$^+$ OCLs of wild-type or *Atp6i*$^{-/-}$ mice for *Atp6i* expression by northern-blot analysis with an α-^{32}P-labelled fragment of 2.6-kb human *Atp6i* cDNA as described[10].

Histological and radiographic procedures. For histological analysis, bones were fixed in 4% paraformaldehyde overnight and decalcified in EDTA (0.5 M, pH 7.4) for 7–10 d at 4 ºC, dehydrated in ethanol and embedded in paraffin. We stained serial sections (5 μm) with haematoxylin and eosin according to standard procedures. The expression of Atp6i in wild-type or *Atp6i*$^{-/-}$ osteoclasts was investigated by immunostaining newborn mouse tibia with an Atp6i-specific polyclonal antibody, which was raised against a peptide corresponding to Atp6i aa 689–695 as described[20]. We carried out TRAP staining using a commercial kit (Sigma) according to the manufacturer's instructions. For X-ray analysis, radiography was performed using a high-resolution, soft X-ray system at 30 kV and high-speed holographic film (Kodak).

Assessment of osteoclast-mediated extracellular acidification. We generated wild-type and *Atp6i*$^{-/-}$ OCLs as described[10]. Briefly, wild-type and *Atp6i*$^{-/-}$ spleen cells were co-cultured with MS12 stromal cells in the presence of vitamin D_3 (10^{-8} M) for 9 d in 24-well plates. TRAP$^+$ OCLs derived from spleen cells were enriched by incubation with 0.2% trypsin for 4 min. The enriched OCLs were then detached with a plastic scraper after treatment with 0.05% trypsin and 0.02% EDTA and pipetted onto dentin slices for OCL acidification assays. Acid production by OCLs generated from wild-type or *Atp6i*$^{-/-}$ mouse spleens was determined using acridine orange[2,10]. Wild-type and *Atp6i*$^{-/-}$ OCL preparations were placed on dentin slices and incubated for 3 h in a CO_2 incubator. They were subsequently incubated in α-minimum essential medium (α-MEM) containing acridine orange (5 μg/ml; Sigma) for 15 min at 37 ºC, washed and chased for 10 min in fresh media without acridine orange. We observed acid production under a fluorescence microscope with a 490-nm excitation filter and a 525-nm arrest filter. We measured acid-base balance in blood and urine of four-week-old mutant and wild-type mice using microelectrodes (Microelectrodes). Data were statistically evaluated by paired *t*-tests.

Immunofluorescence confocal microscopy. We stained wild-type and *Atp6i*$^{-/-}$ OCLs with acridine orange and immunocytochemical staining using a monoclonal antibody against lysosome-associated membrane protein (LAMP-1) on cover slips, sequentially. We found that on the glass surface of cover slips the extracellular acidification compartments formed infrequently compared with culture on dentin slices. This allowed observation of intracellar acidification compartments. After fixation, paraformaldehyde was washed off in three rinses with PBS. We detected LAMP-1 using a rat anti-mouse LAMP-1 monoclonal antibody (1D4B, hybridoma supernatant; Developmental Studies Hybridoma Bank). The hybridoma supernatant was diluted (1:20) in RPMI 1640 followed by Cy5-conjugated affinity-purified goat anti-rat Ig (2.9 μg/ml; Jackson ImmunoResearch Laboratories). We used a Bio-Rad MRC-1024 confocal imaging system equipped with a krypton-argon laser (BioRad Laboratories) and a Nikon inverted microscope with a ×60 objective for laser scanning confocal microscopy.

pH measurements of isolated lysosomes. We determined the internal pH of isolated lysosomes loaded with pH-sensitive FITC-dex as described[12]. Briefly, mice were injected intraperitoneally with FITC-dex (2 mg of FITC-dex/15 g of body weight), starved for 12 h and then sacrificed. The liver homogenate was made in three volumes of sucrose buffer (0.25 M sucrose, 1 mM EDTA, 0.1% ethanol) by a single up-and-down stroke of a Teflon pestle and were fractionated by differential centrifugation as described[12]. We resuspended the final precipitate (lysosome-rich fraction) in sucrose buffer. The lysosome-rich fraction was added to 3 ml of incubation mixture (100 mM KCl, 10 mM $MgCl_2$, 20 mM Hepes/KOH, pH 7.0), and the fluorescence was measured with excitation at 495 nm and emission at 550 nm at 25 ºC on an SPF 125 fluorescence spectrophotometer (American Instrument). Fluorescence was calibrated using the calibration curve as described for lysosomal pH determinations[12].

Microsomal proton transport assay. We prepared microsomes from kidneys of wild-type or *Atp6i*$^{-/-}$ mice as described[13]. Briefly, after removing the capsule, the tissue was minced and diluted with cold homogenization buffer (20 mM HEPES-KOH, 1 mM EDTA, 2 mM dithiothreitol, 250 mM sucrose, pH 7.4, at 4 ºC). Homogenization was performed using a Teflon homogenizer. We centrifuged the homogenate for 7 min at 7,000 r.p.m. in an SS-34 Beckman rotor at 4 ºC. The pellet was discarded, and the supernatant was centrifuged for 40 min at 18,000 r.p.m. in the same rotor. The supernatant was discarded, and the pellet contained a dark tightly packed center covered with white fluffy membrane. The fluffy layer, containing the kidney-derived microsomes, was removed and resuspended in homogenization buffer. Protein determination was done using a protein assay kit (Biorad), with bovine serum albumin as a standard.

We performed the proton transport assay as described[13]. We incubated kidney-derived membrane vesicles (40 μg) for 7 min in 2 ml acidification buffer (150 mm KCl, 20 mm HEPES-KOH, 5 mm MgCl, pH 7.4, 5 μm acridine orange, 1.25 μm valinomycin) at 25 ºC. Proton transport was initiated by addition of potassium ATP and monitored as fluorescence quench of acridine orange (excitation 490 nm, emission 520 nm) using a SPF 125 fluorescence spectrophotometer (American Instrument). The initial rate (ΔF/min) was derived from the slope generated by the first 30 s of the acidification assay. We also determined the total fluorescence change after addition of 1.5 μm nigericin (ΔF).

Acknowledgements

We thank D. Hay, S. Orlando and L.J. Maltais for critical reading of the manuscript; W. Deng for assistance with the manuscript; J. Dobeck for histological assistance; and R. Kent and S.-I. A. Liao for statistical analysis assistance. This work was supported by NIH grants DE-07378 (P.S.) and AR44741 (Y.-P.L.).

Received 7 April; accepted 29 October 1999.

1. Vaes, G. On the mechanisms of bone resorption. The action of parathyroid hormone on the excretion and synthesis of lysosomal enzymes and on the extracellular release of acid by bone cells. *J. Cell Biol.* **39**, 676–697 (1968).
2. Baron, R., Neff, L., Louvard, D. & Courtoy, P.J. Cell-mediated extracellular acidification and bone resorption: evidence for a low pH in resorbing lacunae and localization of a 100-kD lysosomal membrane protein at the osteoclast ruffled border. *J. Cell Biol.* **101**, 2210–2222 (1985).
3. Blair, H.C. & Schlesinger, P.H. in *Biology and Physiology of the Osteoclast* (eds Rifkin, B.R. & Gay, C.V.) 259–287 (CRC Press, Boca Raton, Florida, 1992).
4. Li, Y.P., Chen, W. & Stashenko, P. Molecular cloning and characterization of a putative novel human osteoclast-specific 116-kDa vacuolar proton pump subunit. *Biochem. Biophys. Res. Commun.* **218**, 813–821 (1996).
5. Gerritsen, E.J. *et al*. Autosomal recessive osteopetrosis: variability of findings at diagnosis and during the natural course. *Pediatrics* **93**, 247–253 (1994).
6. Wang, Z.Q. *et al*. Bone and haematopoietic defects in mice lacking c-fos. *Nature* **360**, 741–745 (1992).
7. Tondravi, M.M. *et al*. Osteopetrosis in mice lacking haematopoietic transcription factor PU.1. *Nature* **386**, 81–84 (1997).
8. Iotsova, V. *et al*. Osteopetrosis in mice lacking NF-κB1 and NF-κB2. *Nature Med.* **3**, 1285–1289 (1997).
9. Soriano, P., Montgomery, C., Geske, R. & Bradley, A. Targeted disruption of the c-src proto-oncogene leads to osteopetrosis in mice. *Cell* **64**, 693–702 (1991).
10. Chen, W. & Li, Y.P. Generation of mouse osteoclastogenic cell lines immortalized with SV40 large T antigen. *J. Bone Miner. Res.* **13**, 1112–1123 (1998).
11. Zimmerli, S. *et al*. Phagosome-lysosome fusion is a calcium-independent event in macrophages. *J. Cell Biol.* **132**, 49–61 (1996).
12. Ohkuma, S., Moriyama, Y. & Takano, T. Identification and characterization of a proton pump on lysosomes by fluorescein-isothiocyanate-dextran fluorescence. *Proc. Natl Acad. Sci. USA* **79**, 2758–2762 (1982).
13. David, P. & Baron, R. The catalytic cycle of the vacuolar H(+)-ATPase. Comparison of proton transport in kidney- and osteoclast-derived vesicles. *J. Biol. Chem.* **269**, 30158–30163 (1994).
14. Horton, W.A. The biology of bone growth. *Growth Genet. Horm.* **6**, 1–3 (1990).
15. Johansson, N. *et al*. Collagenase-3 (MMP-13) is expressed by hypertrophic chondrocytes, periosteal cells, and osteoblasts during human fetal bone development. *Dev. Dyn.* **208**, 387–397 (1997).
16. Li, E., Bestor, T.H. & Jaenisch, R. Targeted mutation of the DNA methyltransferase gene results in embryonic lethality. *Cell* **69**, 915–926 (1992).
17. Laird, P.W. *et al*. Simplified mammalian DNA isolation procedure. *Nucleic Acids Res.* **19**, 4293 (1991).
18. Tamura, T. *et al*. New resorption assay with mouse osteoclast-like multinucleated cells formed in vitro. *J. Bone Miner. Res.* **8**, 953–960 (1993).
19. Shibutani, T. & Heersche, J.N. Effect of medium pH on osteoclast activity and osteoclast formation in cultures of dispersed rabbit osteoclasts. *J. Bone Miner. Res.* **8**, 331–336 (1993).
20. Li, Y.P. & Chen, W. Characterization of mouse cathepsin K gene, the gene promoter, and the gene expression. *J. Bone Miner. Res.* **14**, 487–499 (1999).